JAAS

Accepted Manuscript

This is an *Accepted Manuscript*, which has been through the Royal Society of Chemistry peer review process and has been accepted for publication.

Accepted Manuscripts are published online shortly after acceptance, before technical editing, formatting and proof reading. Using this free service, authors can make their results available to the community, in citable form, before we publish the edited article. We will replace this *Accepted Manuscript* with the edited and formatted *Advance Article* as soon as it is available.

You can find more information about *Accepted Manuscripts* in the Information for Authors.

Please note that technical editing may introduce minor changes to the text and/or graphics, which may alter content. The journal's standard Terms & Conditions and the Ethical guidelines still apply. In no event shall the Royal Society of Chemistry be held responsible for any errors or omissions in this *Accepted Manuscript* or any consequences arising from the use of any information it contains.

ROYAL SOCIETY OF CHEMISTRY

www.rsc.org/jaas

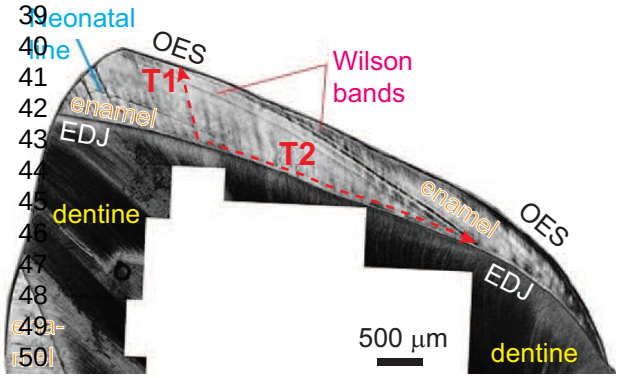

Fig. 1

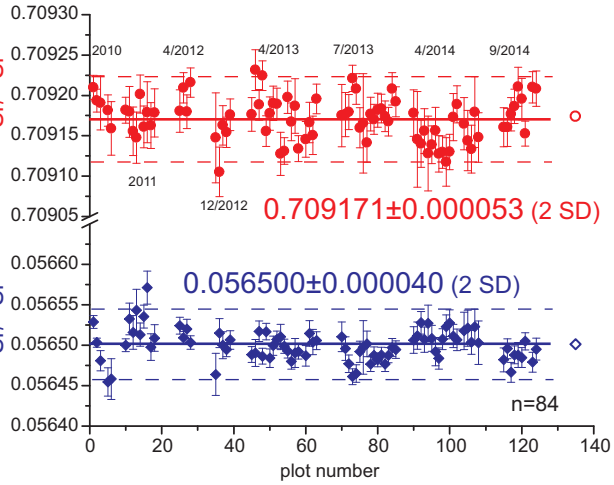

Fig. 2

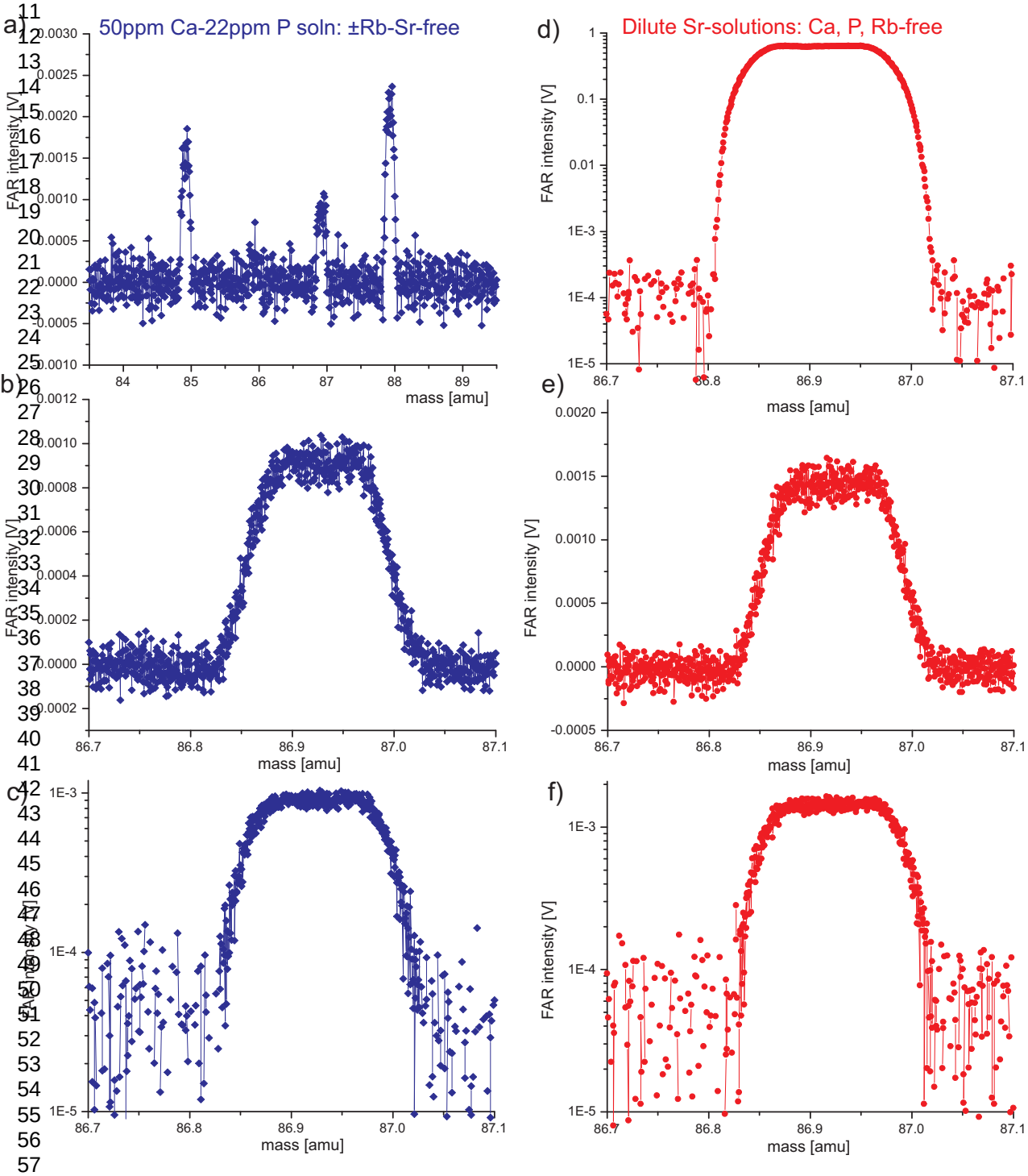

Fig. 3

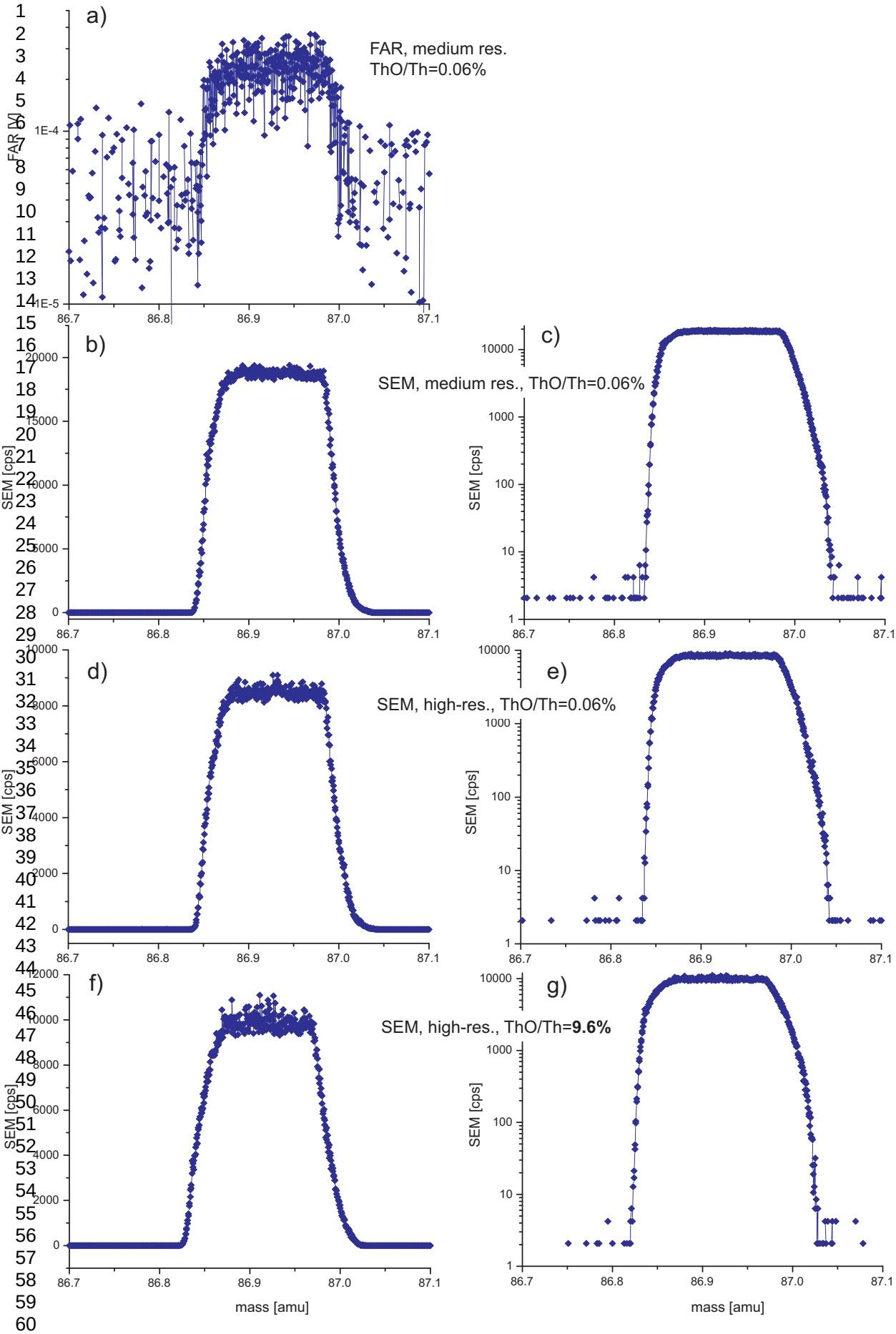

Fig. 4

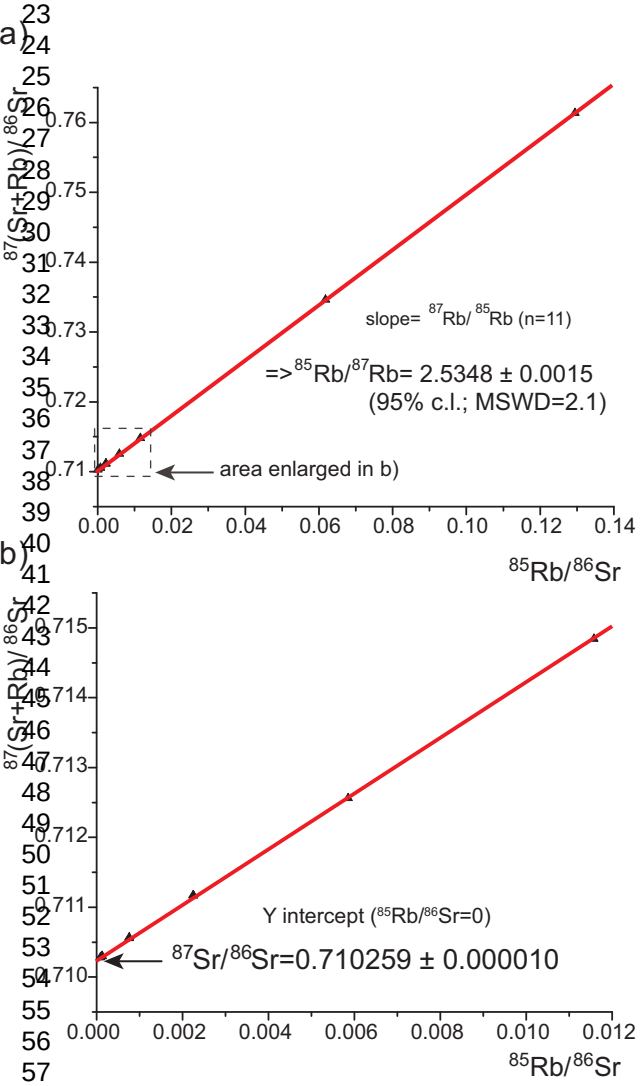

Fig. 5:

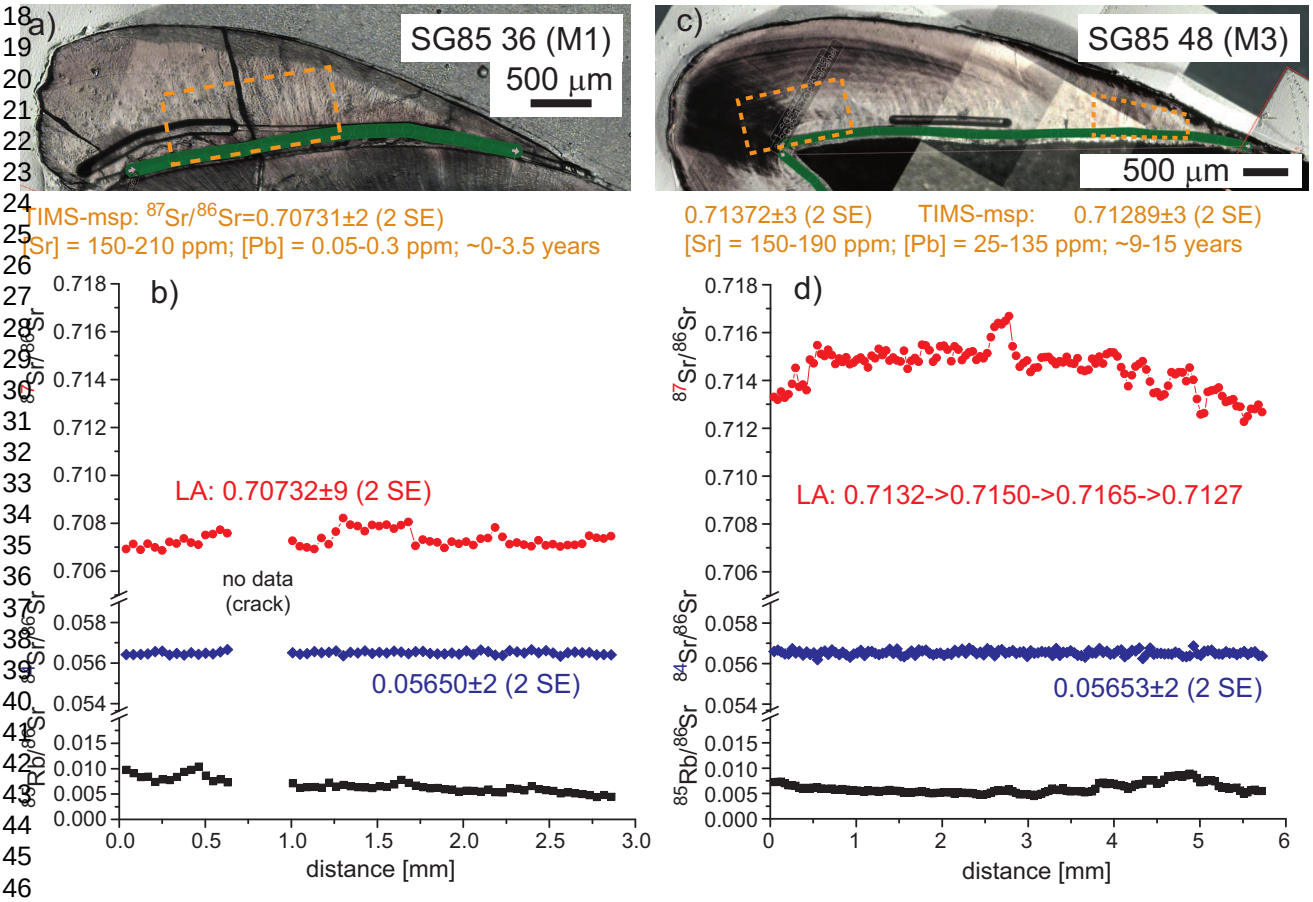

Fig. 6

List of figures (accompanying Müller & Anczkiewicz)

Fig. 1: Transmitted-light thin section photomicrograph of a slightly worn deciduous human canine showing inner dentine being surrounded on the outside by dense enamel. Incremental growth lines within enamel called Retzius lines delineating isochronous layers are visible, of which the more strongly expressed Neonatal line and Wilson bands reflect stress events (e.g. birth, illness).Two main hypothetical laser-ablation tracks (T1, T2) in enamel growth direction are indicated that traverse from earlier to later mineralized enamel, thus potentially allowing extraction of time-resolved elemental/isotopic data: T1 goes across the enamel thickness parallel to enamel prisms from EDJ (enamel-dentine-junction) towards OES (outer enamel surface), whereas T2 runs along the EDJ. Our data follow the T2 track orientation.

Fig. 2: Long-term Sr-isotope ratios of two modern shark in-house reference samples analyzed by LA-MC-ICPMS interchangeably over four years (Aug. 2010 – Sep. 2014; n=84 of 88). Both $^{87}Sr/^{86}Sr$ and $^{84}Sr/^{86}Sr$ ratios yield good long-term reproducibility and resultant averages demonstrate remarkable accuracy as they agree well with modern marine $^{87}Sr/^{86}Sr$ (0.709175 ± 0.000019) and natural $^{84}Sr/^{86}Sr$ ratios (0.056492 ± 0.0000016)[28, 31] (open symbols on right hand side).

Fig. 3: Mass scan (mssc) experiments at low mass-resolution to evaluate the presence of molecular interference $^{40}Ca^{31}P^{16}O$ at m/z=87 (Faraday collector). Results of a ±Rb-Sr-free, concentrated Ca-P solution (a-c) designed to simulate LA apatite analysis are compared to Sr-standard solutions at different concentrations (d-f; all at ThO^+/Th^+=0.06%). Scans are plotted on both linear and logarithmic y-axes, the latter to emphasize the presence of potentially-present, minor peaks slightly offset towards higher masses. Very little, if any, residual non-($^{87}Rb+^{87}Sr$) remain at m/z=87 after Rb-Sr peak stripping (see text; steps: 800, integration time/step: 0.26 s (a), 1.04 s (b, c =same mssc), 0.52 s (e, f =same mssc)).

Fig. 4: Mass scan experiments using a ±Rb-Sr-free, concentrated Ca-P solution at (pseudo)medium (a-c) and (pseudo)high mass-resolution (d-g) to evaluate the presence of molecular interference $^{40}Ca^{31}P^{16}O$ at m/z=87. In view of the small residual signals, Faraday (a) or SEM collectors (b-g) were used. 'Robust' plasma conditions (ThO/Th=0.06%, a-e) vs. deliberately detuned, high oxide plasma conditions (ThO/Th=9.6%, f, g) reveal neither differences in peak-shape, nor, crucially, any minor peaks offset towards slightly higher mass that would indicate molecular interferences. This suggests that $^{40}Ca^{31}P^{16}O$ does not occur at the required intensities to explain offsets in LA-MC-ICPMS $^{87}Sr/^{86}Sr$ ratios of apatite[11, 12]. (see text; steps: 800, integration time/step: SEM 0.52 s, FAR 1.04 s).

Fig. 5: Results for a concentrated Ca-P solution emulating LA-analysis of apatite to which variable amounts of SRM984 (Rb) and SRM987 (Sr) were added, plotted as $^{85}Rb/^{86}Sr_{measured}$ vs. $^{87}(Sr+Rb)/^{86}Sr_{Sr\text{-}mass\text{-}bias\text{-}corrected}$. A remarkably linear regression over a large Rb/Sr range, in fact slightly beyond that of typical natural (bio)apatite ($^{85}Rb/^{86}Sr < \sim 5x10^{-2}$), corresponds to $^{85}Rb/^{87}Rb = 2.5348 \pm 0.0015$ (MSWD=2.1), used subsequently for the effective, mass-bias-adjusted ^{87}Rb-interference correction on ^{87}Sr during LA-MC-ICPMS analyses. The accurate $^{87}Sr/^{86}Sr$ ratio for SRM987 defined by the y-axis intercept demonstrates the robustness of the correction even for highly Rb enriched samples (see text).

Fig. 6: Comparative LA-MC-ICPMS Sr-isotope profiles (green tracks parallel to EDJ) for two teeth of the same individual from the medieval Pb-Ag mining community of Sulzburg (SW Germany; early and late mineralizing M1 & M3). Strongly different inter/intra-enamel $^{87}Sr/^{86}Sr$ values by LA despite elevated $^{85}Rb/^{86}Sr$-values compare well with equivalent microsampling-TIMS data (the dashed polygons indicate their approximate location), even though especially the M3 profile makes reliable comparison unattainable due to the different sample volumes analysed. Corresponding $^{84}Sr/^{86}Sr$ ratios are both accurate and spatially invariant and further support the reliability of the LA data. Not labelled tracks were used for pre-ablation conditioning or earlier trace element analyses. Errors refer to the last digit of the corresponding isotope ratio. See text for details.

Table 1: Dry-plasma operating conditions of MC-ICPMS in both solution-mode (Aridus) and laser-ablation (LA) mode (see text for details).

MC-ICPMS: Neptune	
RF power	Soln.: 1250-1350 W; LA: 1150-1250 W
Sampler, skimmer cones	Normal, not Xcone
Carrier, sweep gas flow (Ar); diatomic gas flow (N_2)	**Aridus II:** PFA nebulizer, 50 µl/min uptake, ~0.89 l/min carrier gas, ~3.5 l/min sweep gas, ~10 ml/min N_2 (all optimized daily) **LA:** ~520 ml/min (optimized daily) ~6.5 ml/min N_2 (optimized daily)
Coolant gas flow	15 l/min
Auxilliary gas flow	0.9 l/min
ThO^+/Th^+ (248/232)	Solution: <0.1 % (typically 0.06 %); LA: <0.2 %
$^{232}Th/^{238}U$	Solution & LA: >0.93
Er^{2+}/Er^+; Yb^{2+}/Yb^+	0.7; 0.4%
Integration time	8 or 4x 1.04 s

Laser-ablation system RESOlution M-50	
Energy density (fluence) on target	8 J/cm^2
LA cell	Laurin two-volume M-50 cell
He gas flow	900 ml/min
Laser repetition rate	5 – 30 Hz
Laser spot size	60 - 110 µm
Ablation mode:	Path ablation, X-Y stage speed 0.3 – 0.5 mm/min
Transport tubing	Nylon
Signal smoothing	Squid included

Table 2: Faraday cup configuration utilized for all Neptune MC-ICPMS analyses; six cups are positioned at nominal full masses, whereas two are placed at half masses to monitor doubly-charged REEs. Besides the Sr and Rb isotopes, the main potential spectral interferences are listed including their approximate isotope abundances (in case of CaCa, CaAr and CaPO only the minor isotopes are listed)[50].

Faraday cup	**L3**	**L2**	**L1**	**C**	**H1**	**H2**	**H3**	**H4**
Element/ isotope (m/z)	82	83.5	84	85	86	86.5	87	88
Sr			84 (~0.56%)		86 (~9.9%)		87 (~7.0%)	88 (~82.6%)
Rb				85 (72.2%)			87 (27.8%)	
Kr	82 (11.6%)		84 (57.0%)		86 (17.3%)			
^{xx}Ca^{40}Ar, ^{xx}Ca^{40}Ca, (^{40}Ca: 96.941%, ^{40}Ar: 99.60%)	^{42}CaAr, ^{42}CaCa (0.647%)		^{44}CaAr, ^{44}CaCa (2.086%)		^{46}CaAr, ^{46}CaCa (0.004%)			^{48}CaAr, ^{48}CaCa (0.187%)
REE^{2+}	^{164}Dy (28.18%), ^{164}Er (1.61%)	^{167}Er (22.93%)	^{168}Er (26.78%), ^{168}Yb (0.13%)	^{170}Er (14.93%), ^{170}Yb (3.04%)	^{172}Yb (21.83%)	^{173}Yb (16.13%)	^{174}Yb (31.83%), ^{174}Hf (0.16%)	^{176}Yb (12.76%), ^{176}Hf (5.26%), ^{176}Lu (2.59%)
CaPO							^{40}Ca^{31}P^{16}O (^{16}O: 99.76%)	^{40}Ca^{31}P^{17}O (^{17}O: 0.038%)

50. K. J. R. Rosman and P. D. P. Taylor, *J. Anal. At. Spectrom.*, 1998, **13**, 45N-55N

Manuscript ID: JA-ART-07-2015-000311

Müller & Anczkiewicz: Accuracy of Laser-Ablation (LA)-MC-ICPMS Sr Isotope Analysis of (Bio)Apatite – a Problem Reassessed

Table of Contents entry:

Accurate in-situ Sr isotope analysis of (bio)apatite via 'robust-plasma' laser-ablation MC-ICPMS with negligible $^{40}Ca^{31}P^{16}O$ and reliable ^{87}Rb interference correction

Journal Name

ARTICLE

Accuracy of Laser-Ablation (LA)-MC-ICPMS Sr Isotope Analysis of (Bio)Apatite – a Problem Reassessed

Received 00th January 20xx,
Accepted 00th January 20xx

DOI: 10.1039/x0xx00000x

www.rsc.org/

Wolfgang Müller[a] and Robert Anczkiewicz[b]

Apatite is a key mineral whose Sr-isotope record has a wide range of applications including palaeofluid flow studies from inorganic apatite, and past faunal/human mobility or palaeoecology using bioapatite. The incremental growth of mammalian enamel bioapatite potentially allows extraction of Sr isotopic compositions at sub-annual time-resolution using laser-ablation plasma mass spectrometry (LA-MC-ICPMS). However, existing apatite LA-MC-ICPMS Sr-isotope data have yielded mixed results. Here we assess the achievable accuracy/precision of (bio)apatite LA-MC-ICPMS Sr-isotope analysis and evaluate sources of inaccuracy. Using robust plasma conditions (ThO^+/Th^+<0.2%), we obtain long-term (4 year) accurate and precise Sr-isotope data for modern shark teeth for both radiogenic $^{87}Sr/^{86}Sr$ (0.709171±0.000053, 2 SD), and naturally invariant $^{84}Sr/^{86}Sr$ (0.056500±0.000040, 2 SD). Based on our accurate $^{84}Sr/^{86}Sr$-results also for low-Sr enamel, we deduce that interferences are successfully corrected (Kr) or negligible (Ca-argide/dimer), leaving ^{87}Rb and $^{40}Ca^{31}P^{16}O$ isobaric interferences as key potential sources for $^{87}Sr/^{86}Sr$ inaccuracy. Our (pseudo)high-resolution mass scans using a virtually Rb-Sr-free, concentrated Ca-P-solution simulating apatite LA analysis show no evidence for $^{40}Ca^{31}P^{16}O$ at the required intensities to explain previously observed $^{87}Sr/^{86}Sr$ offsets. Rather, using the same Ca-P solution with varying Rb+Sr isotope standard additions, we accurately constrain the mass bias-corrected $^{85}Rb/^{87}Rb$-ratio, and using apatite glasses assess the extent of Rb/Sr elemental fractionation during laser-ablation. Finally, we present concordant LA-MC-ICPMS and microsampled-TIMS $^{87}Sr/^{86}Sr$ results for low-Sr tooth enamel with highly variable inter&intra-$^{87}Sr/^{86}Sr$ ratios and comparatively high Rb/Sr-ratios. This archaeological example also illustrates well the problem of defining equivalent sample volumes that allow unequivocal comparison between LA and TIMS data.

1) Introduction

The (Rb-)Sr system is particularly well-suited for *in-situ* isotopic analysis. This is due to (1) the occurrence of large natural Sr-isotopic variations resulting from the strongly contrasting geochemical behaviour of Rb and Sr coupled with the radioactive decay of ^{87}Rb to ^{87}Sr, (2) the high Sr yet concomitantly low Rb concentrations found in a variety of materials due to the geochemical resemblance of Sr with major element Ca, and (3) the ubiquitous occurrence of Sr-rich minerals (e.g. feldspars, apatite, clinopyroxene), rocks (carbonates, phosphates) or biological materials (e.g. otoliths, teeth).

In-situ analysis at high-spatial resolution is essential in order to extract the time-series information at high resolution stored in continuously growing samples like otoliths, dental enamel or speleothems and/or to retrieve isotopic information with textural control (e.g in zoned plagioclase). Besides the much improved spatial resolution compared to conventional microsampling [1, 2], *in-situ* analysis is also faster than thermal ionization mass spectrometry (TIMS) or solution multi-collector inductively-coupled-plasma mass spectrometry (MC-ICPMS), but at the expense of not being able to chemically remove isobaric interferences off-line via ion-exchange chemistry.

The potential of *in-situ* Sr isotope analysis using laser-ablation-MC-ICPMS (LA-MC-ICPMS) with precision comparable to TIMS was realized early in the development of MC-ICPMS[3]. Consequently, LA-MC-ICPMS Sr-isotope analyses applied to carbonates or feldspars have gradually become standard methodological repertoire[4-7], despite the occasionally reported accuracy problems[8, 9]. On the other hand, LA-MC-ICPMS Sr isotope investigations of inorganically or biologically formed *Ca-phosphates (apatite)* have often resulted in inaccurate data, attributed to the existence of an interference on m/z=87 from $^{40}Ca^{31}P^{16}O$ [10-12], even though some successful applications also have been reported, albeit with somewhat reduced precision/accuracy [13, 14]. Apatite is not only a key inorganic mineral recording, for example, palaeo-fluid flow processes[15], but it is especially also the key biomineral in vertebrate skeletons. The Sr-isotopic composition particularly of tooth enamel has arguably become the key methodology in palaeoecology and archaeology to trace past faunal or human

[a] Department of Earth Sciences, Royal Holloway University of London, Egham, UK. (wolfgang.muller@rhul.ac.uk)
[b] Institute of Geological Sciences, Polish Academy of Sciences, Krakow, Poland.
[c]

† Footnotes relating to the title and/or authors should appear here.
Electronic Supplementary Information (ESI) available: [details of any supplementary information available should be included here]. See DOI: 10.1039/x0xx00000x

mobility[16, 17]. Owing to the incremental two-stage mineralization[18, 19] of tooth enamel over several years, for example in humans of ~15 years, spatially-resolved Sr-isotopic data of enamel have the potential to reveal sub-seasonal mobility patterns, especially if combined with counted chronologies from enamel histology[20] (Fig. 1).

Here we report the results of systematic investigations aimed at evaluating the various sources of inaccuracy of LA-MC-ICPMS $^{87}Sr/^{86}Sr$ ratio analysis of (bio)apatite, focusing on radiogenic variability rather than natural stable Sr-isotope variations. Besides reporting accurate values of the naturally invariant $^{84}Sr/^{86}Sr$ ratio (if normalized to constant $^{88}Sr/^{86}Sr$[21]), we focus on the presence of $^{40}Ca^{31}P^{16}O$ signals via detailed mass scans at various mass resolutions, because at m/z=87, molecular interferences such as $^{40}Ca^{31}P^{16}O$ are resolvable from either ^{87}Sr or ^{87}Rb at medium or high mass resolution. We also assess the crucial ^{87}Rb correction, the accuracy of which for (bio)apatite is paramount in view of the often elevated $^{85}Rb/^{86}Sr$ ratios (~$5x10^{-2}$ to 10^{-4}). Finally, we show not only long-term (~4 year) external standard reproducibilities of Sr-isotope ratios by LA-MC-ICPMS, but importantly also results of comparative microsampling-TIMS vs. LA-MC-ICPMS analyses of the same archaeological human teeth to evaluate accuracy of the latter.

2) Materials and Methods

All Sr isotopic data – both in solution and laser-ablation mode - were obtained in dry-plasma mode using a ThermoFisher Neptune MC-ICPMS at the Institute of Geological Sciences, Krakow Research Centre of the Polish Academy of Sciences. The MC-ICPMS is either coupled with an Aridus II desolvating nebulizer (Cetac) or a RESOlution M-50 excimer (193 nm) laser-ablation system (Resonetics, now Australian Scientific Instruments (ASI); Tab. 1). The latter features a two-volume Laurin LA cell which ensures signal uniformity as well as rapid washout anywhere in the cell[22]. Eight of the nine Neptune Faraday (FAR) cups equipped with 10^{11} Ω resistors were used for static analysis; L4 could not be utilized due to its limited mobility caused by the attached block of four ion counters (Tab. 2). Faraday cups L2 and H2 were placed at half mass positions (nominal m/z=83.5 and 86.5) using both Er-Yb doped Rb-Sr solutions and LA of Durango apatite to monitor the presence of REE^{2+} since diagenetically-modified bioapatite may contain appreciable REE concentrations[23]. Cup efficiencies were set to unity, and gain of amplifiers measured at least once daily. Mass scan experiments utilized either the axial FAR detector or the axial secondary electron multiplier (SEM) detector. All Neptune LA data were obtained in low mass resolution (ΔM/M = 400), whereas some solution experiments, especially regarding mass scans, were conducted at (pseudo)medium and (pseudo)high mass resolution (ΔM/M = 4000, 10000, respectively). Peak centering was done at the start of an analysis and was found to be extremely stable. In order to accurately correct for Kr isobars (typical ^{84}Kr-signals ~0.3–0.45 mV; ~1-1.5% of ^{84}Sr) and all other baseline signals, extended (2x 90 s) on-peak background measurements were used. In order to have an isotopic match for the on-peak baseline measurement, a quick (1-2 mins) 'pre-ablation' of the material to be analyzed preceded the baseline measurements following signal washout. Data were collected in cycles each comprising four or eight 1.05 s integrations. Peak intensities were corrected online for baseline contributions, exported and all further data reduction was done offline. Exponential mass bias correction using constant $^{88}Sr/^{86}Sr$[21] was applied following offline peak-stripping using custom data reduction in EXCEL. Doubly-charged Er and Yb signals were monitored but found to be negligible for both standards and samples analyzed herein because modern and well-preserved fossil/archaeological teeth are characterized by [REE] in the (sub-)ppb concentration range[23].

Additional contextual LA-ICPMS trace element concentration data were obtained at Royal Holloway University of London (RHUL) using the RESOlution M-50 prototype LA system featuring a Laurin two-volume LA cell coupled to an Agilent 7500ce quadrupole-ICPMS[22].

Emphasis of both solution and LA-MC-ICPMS analyses was on 'robust' plasma conditions characterized by very low ThO^+/Th^+-ratios (<0.2%; unless deliberately detuned, see below) and $^{232}Th/^{238}U$-ratios >0.93 (solutions with equal Th-U concentrations or SRM612), which were achieved by attention to carrier gas flow, RF power and aided by using a dry plasma with N_2-addition[24, 25] (Tab. 1). We note that ThO^+ represents the maximum metal oxide-production owing to its highest metal-oxygen bond strength[26-30], and that other common oxide-production monitoring ratios (e.g. UO^+/U^+ [31] and CeO^+/Ce^+) are ~2.5-3.5x lower. With the exception of the alkali-metals, this is valid not only for neutrals but also for metal-cations because the corresponding metal-O or metal-cation-O bond strengths differ by no more than ±10-20% [26, 27, 30]. Er^{2+} and Yb^{2+} production rates were 0.7 and 0.4%, respectively. Overall, conditions were kept as similar as possible between the two modi so as to allow comparability of the corresponding results. X-geometry skimmer cones were not used due potentially elevated oxide production that is offset only with minimal (<10%) sensitivity gain[32].

2A) Solution MC-ICPMS analysis

Solution analysis was designed such that it simulated LA analysis of apatite as closely as possible, especially regarding the presence of Ca and P ions to obtain equivalent mass bias data for the correction of LA analyses. Based on the Sr sensitivity of ~140 V/ppm for above tuning conditions, 50 ppb Sr yield ~7 V Sr_{total} (5.8 V ^{88}Sr), which also constitutes a Sr-signal for suitably precise LA-MC-ICPMS isotope analysis (ideally >1.5 V ^{88}Sr). Considering bioapatite stoichiometry characterized by both Ca/P-ratios of ~2.15 and Sr/Ca ratios between $3x10^{-4}$ to $3x10^{-3}$ (equivalent to [Sr] 100-1000 ppm), we prepared a 50 ppm - 22 ppm Ca-P solution from 1000 ppm single element ICP/AAS standard solutions. Residual Rb and Sr impurities were removed from this Ca-P solution via two-stage ion exchange chemistry using cation resin AG50W-X8 (BioRad) and SrSpec resin[33] (Eichrom). This Ca-P-solution was used for

all mass scan experiments as well as the experiments to assess the prevailing $^{85}Rb/^{87}Rb$-ratio for accurate Rb-correction via variable SRM987/SRM984 (Sr/Rb) additions (see below). Detailed conditions such as integration time, detector type, mass resolution of the mass scans are given where applicable.

2B) Laser-Ablation-MC-ICPMS analysis

Using an energy density on the sample surface of ~8 J/cm^2, laser-ablation took place in a He atmosphere (~900 ml/min flowrate through LA cell), with Ar and N_2 (~520, ~6.5 ml/min, respectively; all optimized daily) being admixed downstream of the ablation cell before the squid signal smoothing device[22] (Tab. 1). All LA data acquisition took place in continuous path ablation mode. Depending on analyte Sr concentration and the desired spatial resolution, laser spot and repetition rate were selected and ranged between 60-110 µm and 5-30 Hz, respectively, with target ^{88}Sr signals in LA mode ranging between ~2 – 8 V.

Tuning for maximum sensitivity and signal stability as well as best peak shape while maintaining above mentioned robust plasma characteristics was performed in path ablation mode using SRM616 glass (41.7 ppm Sr[34]), which yielded 0.8–1.8 mV/ppm ^{88}Sr using a 60 µm spot, 5 Hz repetition rate and 1 mm/min stage speed, depending on cones and prior usage. SRM616 with its low Rb/Sr ratio (0.0025) was chosen so as to avoid unnecessary Rb build-up on cones, crucial in view of maintaining accurate on-peak baselines. Using the higher concentrated NIST-glasses (SRM612, 610) can lead to increasing Rb-signals due to 'cone-erosion'; the latter, however, were used briefly to assess $^{232}Th/^{238}U$ and ThO^+/Th^+-ratios. Matrix-matched Ca-P-(Si) STDP glasses[35] were used to evaluate elemental Rb/Sr fractionation.

The main in-house Sr-isotope standard used is the isotopically-homogenous (Sr) enameloid of modern shark teeth captured off-shore W-Australia and S-Africa, respectively, with [Sr] of ~2500 µg/g. These record the modern open-marine $^{87}Sr/^{86}Sr$ ratio of 0.709175[36]; whale teeth were evaluated but not utilized further because of their too thin enamel.

2C) Comparative TIMS analysis

Thick sections (~200 µm) were prepared from tooth halves of medieval humans from the small Pb-Ag mining community of Sulzburg (Black Forest, SW Germany)[37, 38] and used for comparative Sr-isotope LA-MC-ICPMS and microsampling-TIMS (msp) analyses. Microsampling of enamel fragments (~160-720 µg) using a microscope-mounted drill followed by conventional TIMS analysis[2, 33] provides comparative data to LA-MC-ICPMS results. The former followed previously published methodology[2, 33] with the exception that analyses utilized a VG354 TIMS in multi-dynamic mode at RHUL[39]. Sr total procedure blanks were 47.4 ± 14.6 pg (1 SD, n=4) and no blank correction was necessary in view of sample Sr contents. Corresponding analyses of SRM987 (≥30 ng) yielded $^{87}Sr/^{86}Sr$ 0.710253 ± 0.000018 (2 SD; n=10).

3) Results and Discussion

All results are listed in Tables 3-5 (ESI) and displayed in Figures 2-6.

3A) LA-MC-ICPMS Sr isotope data of marine Ca-phosphates

The long-term (Aug. 2010 – Sep. 2014) LA-MC-ICPMS reproducibility of both $^{87}Sr/^{86}Sr$ and $^{84}Sr/^{86}Sr$ ratios of two modern shark enameloid specimens serving as in-house reference samples analyzed interchangeably over four years are shown in Fig. 2 and Tab. 3 (ESI). The resultant $^{87}Sr/^{86}Sr$ and $^{84}Sr/^{86}Sr$ ratios are 0.709171 ± 0.000053 (2SD; 0.075 ‰) and 0.056500 ± 0.000040 (2 SD; 0.71 ‰), respectively (n=84 of 88). These values agree well with the modern marine $^{87}Sr/^{86}Sr$ (0.709175 ± 0.000019[36, 39]) and the natural $^{84}Sr/^{86}Sr$ ratios (0.056492 ± 0.0000016[39]). There is no significant trend discernible in either of the two Sr-isotope ratios over the four-year measurement period. Corresponding SRM987 solution data obtained in dry-plasma mode on the same MC-ICPMS during the same time period are 0.710249 ± 0.000014 (2SD) and 0.056494 ± 0.000037 (2 SD; n=48) for $^{87}Sr/^{86}Sr$ and $^{84}Sr/^{86}Sr$, respectively. Our external LA-MC-ICPMS reproducibilities (2SD) of ±0.000053 ($^{87}Sr/^{86}Sr$) and ±0.000040 ($^{84}Sr/^{86}Sr$) are 3.80x and 1.07x larger than the respective solution values, which is interpreted to stem from residual biases from spectral interferences such as ^{87}Rb and $^{84,86}Kr$. The strongly Kr-interference-affected $^{84}Sr/^{86}Sr$-ratio has a comparable precision thus indicating that both solution and LA analyses may be similarly limited by the ability of correcting for $^{84,86}Kr$ that affects both sample introduction modi equally via the Ar plasma gas. On the other hand, the $^{87}Sr/^{86}Sr$ values are almost fourfold less reproducible relative to solution data. We interpret this to reflect that on-peak baselines for the very small ^{85}Rb signals in shark teeth in tandem with slightly varying residual on-peak Rb-memories from e.g. cones may have contributed to the degraded reproducibility (see below). Alternatively, the slightly worse LA vs. solution reproducibility of the $^{84}Sr/^{86}Sr$ ratio (0.05 ‰) may also partially help explain the difference (~0.04 ‰) between the best reported LA $^{87}Sr/^{86}Sr$-isotope ratio reproducibilities (0.000024; 0.035 ‰[4]) and the one observed here (0.00053; 0.075 ‰).

Our LA-MC-ICPMS data of marine bioapatite are remarkably accurate not only for the $^{87}Sr/^{86}Sr$ but especially also the $^{84}Sr/^{86}Sr$ ratio. The latter is a particularly sensitive indicator for the presence of spectral interferences because ^{84}Sr is the least abundant Sr isotope (0.56% abundance), yet interfered not only by the most abundant Kr isotope (^{84}Kr=57.0%) but potentially also the largest Ca-dimer ($^{44}Ca^{40}Ca$) and Ca-argide ($^{44}Ca^{40}Ar$; ^{44}Ca=2.086%). In addition, the denominator-isotope ^{86}Sr is interfered by the second most abundant Kr-isotope (^{86}Kr=17.3% and a small Ca-argide/dimer interference, ^{46}Ca=0.004%). The fact that we routinely obtain accurate $^{84}Sr/^{86}Sr$ data suggests that not only the extended on-peak baselines adequately correct for invariably present $^{84,86}Kr$ (^{84}Kr ~1-1.5% of ^{84}Sr) but also that no resolvable molecular Ca-dimer/argides are present. The latter is further confirmed because m/z=82 (chiefly $^{42}Ca^{40}Ar$, $^{42}Ca^{40}Ca$) typically shows

background-corrected intensities not resolvable from 0 µV (see below for equally accurate $^{84}Sr/^{86}Sr$ ratios of lower-[Sr] human enamel). Other studies, notably with different MC-ICPMS instrumentation, report the presence of significant Ca-Ca/Ar signals[4, 7, 8] affecting especially the $^{84}Sr/^{86}Sr$ ratio, whereas others report no such effects [40, 41]. We surmise that both different plasma sources of MC-ICPMS instruments and especially attention to plasma tuning contribute to this difference, and deduce from our results that the Kr, Ca-dimers/argides (and REE^{2+}) spectral interferences have successfully been corrected herein.

3B) Presence of $^{40}Ca^{31}P^{16}O$ at m/z=87

While the very similar atomic masses of ^{87}Rb and ^{87}Sr (86.9092 and 86.9089 amu, respectively) make mass spectrometric resolution other than via reaction-chemistry[42] essentially impossible, the presence of the potentially interfering Ca-P-O compound can be evaluated because its molecular mass is 0.0224 amu larger than the nuclide masses (86.931 vs. 86.909 amu) and it may form composite peaks akin to e.g. Fe-isotope analysis[43]. Owing to the required mass resolution of ≥3900 (R=ΔM/M), we utilized both (pseudo)medium as well as (pseudo)high mass resolution to assess the presence of this interference. Because no homogenous low-Sr apatite is available for lengthy mass scans in LA mode, we mimicked laser-ablation of apatite using a nearly Rb-Sr-free, concentrated Ca-P solution (50+22 ppm, respectively) in dry-plasma mode (see above). The major element concentration was chosen so as to emulate a bioapatite LA analysis with [Sr] of 100 ppm (Sr/Ca= $3x10^{-4}$, equivalent to ~2 V ^{88}Sr).

Using the central Faraday detector, comparative mass scans at low mass resolution of both the Ca-P solution and clean Sr-solutions are shown in Fig. 3. Based on both residual ^{85}Rb and ^{88}Sr peaks (1.5, 2.0 mV), the contribution of both ^{87}Rb and ^{87}Sr to m/z=87 can be evaluated, which leaves <0.04 mV non-^{87}(Rb+Sr) at m/z=87. This strongly contrasts with the suggestion that 0.3-1% of m/z=87 are Ca-P-O-related[11], implying that for LA apatite analysis yielding 2 V ^{88}Sr (170 mV ^{87}Sr), Ca-P-O should be ~0.5-1.7 mV (>10-45x of what is seen here). Apart from observing identical (residual) m/z=87 peaks for both the Ca-P and the clean Sr solutions (Fig. 3c-f) and quantifying the Rb+Sr contributions, low mass resolution is not sufficient to assess the potential presence of $^{40}Ca^{31}P^{16}O$.

At medium and high mass resolving power (Fig. 4) the residual m/z=87 signals using the Ca-P solution are very small (<0.2 mV) and thus not only FAR but also SEM mass scans are shown. Neither the Faraday nor SEM scans show any evidence for a secondary (molecular) peak offset towards higher mass, even though the MC-ICPMS was also deliberately detuned towards high oxide production (ThO^+/Th^+ ~9.6% vs. typically 0.06%; Fig. 4f, g vs. Fig. 4a-e). Yet even at these unusual plasma conditions, the mass scans are not noticeably different. We note that the SEM scans are not as symmetric as the equivalent FAR scans but crucially show no difference despite >150x varying oxide-levels. Slight peak asymmetry using the SEM is not untypical in our experience also with other elements, but most importantly m/z=87 at (pseudo)high-mass resolution shows a flat peak plateau. We therefore deduce that $^{40}Ca^{31}P^{16}O$ does not occur at the intensities high enough to explain the $^{87}Sr/^{86}Sr$ offsets observed in some cases of LA-MC-ICPMS analysis of apatite[11, 12]. Both Ca and P (and indeed Ca^+ and P^+ cations) are characterized by significantly lower oxygen affinity compared to Th (or Th^+) [26-28, 30], and their oxide production can be approximated from the logarithmic relationship between metal-oxide/metal-ion ratio to M-O bond strength[29]. Plotting our measured log Th^+, U^+ and Ce^+ oxide production relative to the respective bond strengths (bond dissociation energies) facilitates an approximate extrapolation to both Ca^+ and P^+, whose oxide productions become ~0.0007 and ~0.004 %, respectively. It is unclear how likely a more complex triatomic CaPO molecule would form, but it may well form even less likely than Ca-O, in which case the ~0.0007 % value would represent an upper limit, supporting our observation of essentially negligible $^{40}Ca^{31}P^{16}O$ at m/z=87.

3C) Accuracy of ^{87}Rb correction

Apart from the potential of direct online Rb-Sr separation by ETV[44] or reaction cell chemistry[42], the necessary isobaric correction of ^{87}Rb on ^{87}Sr for LA-MC-ICPMS analyses is performed by monitoring isobaric-interference-free ^{85}Rb and applying an appropriate $^{85}Rb/^{87}Rb$-ratio. In contrast to most carbonates with low $^{85}Rb/^{86}Sr$ ratios[4] (~10^{-4}), bioapatite often has elevated $^{85}Rb/^{86}Sr$ ratios between ~$5x10^{-2}$ and 10^{-4} (see below). A $^{85}Rb/^{86}Sr$ ratio of 0.0026 results in a $^{87}Rb/^{86}Sr$ correction of ~0.001 on $^{87}Sr/^{86}Sr$, whose accuracy however depends on the effective $^{85}Rb/^{87}Rb$ and Rb/Sr ratios during analysis.

Using our essentially Rb-Sr-free concentrated Ca-P solution as apatite matrix (see above), we prepared aliquots with varying $^{85}Rb/^{86}Sr$ ratios from $9.1x10^{-5}$ to $1.3x10^{-1}$ by adding varying amounts of SRM984 (Rb) and SRM987 (Sr) while maintaining few tens of ppb [Sr] (Tab. 4 (ESI)). Plotting the Sr-mass-bias-corrected but ^{87}Rb-uncorrected $^{87}(Sr+Rb)/^{86}Sr$-ratio vs. the measured $^{85}Rb/^{86}Sr$ ratio yields the effective $^{87}Rb/^{85}Rb$-ratio as slope and the SRM987 $^{87}Sr/^{86}Sr$-ratio as y-intercept of the regression line. The resultant regression line is highly linear across the considerable range of Rb/Sr-ratios, yielding a slope, converted into $^{85}Rb/^{87}Rb$, of 2.5348 ± 0.0015 (95% c.l., MSWD=2.1, n=11 (MSWD…mean square weighted deviation)) and a y-intercept (0.710259 ± 0.000010), the latter in line with Rb-free SRM987 values (Fig. 5). These values remain indistinguishable within uncertainties if the highest two $^{85}Rb/^{86}Sr$ ratios are excluded ($^{85}Rb/^{87}Rb$ = 2.5265 ± 0.0172 (95% c.l., MSWD=2.0, n=9). As expected from ICP mass bias, the 2.5348 value is lower than the accepted natural $^{85}Rb/^{87}Rb$-ratio (2.59265[45]; -2.24%) and interpreted to represent the $^{85}Rb/^{87}Rb$ ratio necessary for an accurate Rb-mass-bias correction in the presence of large Ca-P ion beams such as during LA-MC-ICPMS analysis of apatite.

We note that there are considerable differences on how to correct for the inevitable isobaric ^{87}Rb amongst the various Sr-isotope LA-MC-ICPMS studies. Some suggest strongly mass

bias affected $^{85}Rb/^{87}Rb$ values of ~2.468[6, 46], others utilize natural-Rb ($^{85}Rb/^{87}Rb$=2.59265) and assume Sr-mass bias to be applicable[31, 41], others use $^{85}Rb/^{87}Rb_{used}$ > $^{85}Rb/^{87}Rb_{natural}$ (2.5970)[13] and in some cases relatively little detail is provided[12, 47]. While this is less important for lowest-Rb/Sr minerals (e.g. carbonates), we want to highlight current inconsistencies whose impact may be particularly important for elevated Rb/Sr-material such as bioapatite (see below).

The extent of elemental fractionation during LA-MC-ICPMS analysis of apatite was assessed using matrix-matched Ca-P-(Si) STDP-glasses[35]. It was found that the 'true'/measured value for Rb/Sr-ratios for the three different STDP-compositions is 1.155±0.023 (1 SD), which is unsurprising given the strong difference in volatility between Rb and Sr[48], affecting the elements differently during condensation from the laser-induced-plasma[49]. Hence we utilize above factor during correction for ^{87}Rb interference and thus also report more accurate sample Rb/Sr ($^{85}Rb/^{86}Sr$) ratios based on LA-MC-ICPMS (Tabs. 3, 5 (ESI)).

3D) Application

From the medieval Pb-Ag mining village of Sulzburg (Black Forest, SW Germany, 12th century AD [37, 38]), well-preserved earliest and late mineralizing molars (M1 and M3) from the same individual were chosen to evaluate the accuracy of LA-MC-ICPMS Sr-isotope results in bioapatite with [Sr] of 150-200 ppm and moderately elevated Rb/Sr ratios typical of mammalian dental enamel. Individual SG85 (adult, female?) was selected because of the strongly contrasting *in-vivo* Pb concentrations revealed by LA-ICPMS[50] in the M1 and M3 enamel, recording Pb-exposure during earliest childhood (~0-3.5 years) and adolescence (~9-15 years)[51], respectively. Tooth enamel grows sequentially and does not remineralize after formation, thus preserving time-series information of changing environmental parameters. The inter- and intra-tooth enamel Pb concentrations of SG85 range between 0.05-0.3 ppm (nearly Pb-unpolluted; M1) and 25-135 ppm (heavily Pb-exposed; M3), respectively, and thus exceed three orders of magnitude for the same individual (a detailed presentation and discussion of the trace element data is beyond the scope of this paper and mentioned here for contextual purposes only). This potentially indicated residential change thus warranting inter&intra-tooth $^{87}Sr/^{86}Sr$ analysis as key mobility proxy, all facilitated by the variable geology at the Rhine graben/Black Forest boundary near Sulzburg. Corresponding comparative microsampling-TIMS and LA-MC-ICPMS analyses are found in Tab. 5 (ESI) and Fig. 6 (it should be noted that this example is shown here for methodological purposes rather than fully discussing all application-specific implications).

In line with the contrasting Pb-concentrations in SG85, strongly different inter&intra-tooth-$^{87}Sr/^{86}Sr$ ratios are recorded for the early and late mineralizing teeth. The 1st molar (SG85-36) has a low $^{87}Sr/^{86}Sr$ ratio of 0.70731 ± 0.00003 (2 SE; TIMS msp, ~720 µg), which compares well with the average from the rather uniform LA-MC-ICPMS profile analyzed in growth direction along the enamel-dentine-junction (EDJ; 0.70732 ± 0.00009; 2 SE). The corresponding $^{84}Sr/^{86}Sr$ ratio is 0.05650 ± 0.00002 (2 SE) and agrees well with the naturally invariant $^{84}Sr/^{86}Sr$ ratio[39]; the $^{85}Rb/^{86}Sr$ ratio decreases slightly from ~0.009 to 0.005.

Two fragments from near occlusal and cervical end of the 3rd molar (SG85-48, M3, wisdom tooth; no data available for the middle fragment) analyzed by TIMS-msp reveal much more radiogenic $^{87}Sr/^{86}Sr$ ratios of 0.71372 ± 0.00003 and 0.71289 ± 0.00003 (2 SE; 350 + 160 µg), respectively. In this case, the comparative LA-MC-ICPMS profile analyzed in growth direction is highly variable and reveals more fine detail. The initial 0.6 mm show $^{87}Sr/^{86}Sr$ values between 0.7132-0.7135, followed by a rapid rise to 0.7150 ± 0.0001 (~2 mm), a further 0.35 mm wide peak (0.7165), before $^{87}Sr/^{86}Sr$ again decreases via a series of 3-4 'wiggles' to 0.7127. Overall the $^{87}Sr/^{86}Sr$ data are in line with the TIMS msp data but this sample illustrates well the problem of defining equivalent volumes that allow unequivocal comparison between TIMS and LA data. Because of the observed intra-enamel variability combined with the complex enamel mineralization process along and across the EDJ (Fig. 1), uncertainties remain which parts to integrate across to obtain the best TIMS-msp value relative the narrow LA track. Despite considerable $^{87}Sr/^{86}Sr$ variability, the corresponding $^{84}Sr/^{86}Sr$ profile is flat throughout recording 0.05653 ± 0.00002, while the $^{85}Rb/^{86}Sr$ ratio varies considerably (0.0073–0.0047–0.0087–0.0055). Despite necessitating a substantial ^{87}Rb-correction on $^{87}Sr/^{86}Sr$, overall the $^{87}Sr/^{86}Sr$ ratio agreement between LA-MC-ICPMS and TIMS-msp for virtually homogenous M1 is excellent (within error) and for variable M3 highly satisfactory (see above); both also record accurate and spatially-invariant $^{84}Sr/^{86}Sr$ ratios.

The local $^{87}Sr/^{86}Sr$ range for Sulzburg can be approximated from both water and diagnetically-altered high-[Sr] bone samples, which are 0.7138 ± 0.0009 and 0.7148 ± 0.0009 (2 SD), respectively[52]. These imply that the lowest-[Pb] childhood Sr-isotopic composition of SG85 (M1) is incompatible with that of mining village, strongly suggesting that individual SG85 was born elsewhere. In contrast, the adolescence $^{87}Sr/^{86}Sr$-range recorded in the M3 agrees with Sulzburg values, implying that SG85 migrated there sometime between ~4 and ~9 years of age and became exposed to high-levels of Pb. The fairly unradiogenic M1 composition suggests carbonate-dominated soils as childhood home, and given the low value of 0.7073 it furthermore hints at Jurassic bedrock compositions[36, 53].

4) Conclusions

On the basis of our laser-ablation and solution experiments and given the rapidly growing significance of spatially resolved Sr-isotope analyses of apatite for a range of applications, we conclude as follows:

1) Our shark-teeth Sr-isotope data obtained by LA-MC-ICPMS over a four-year period demonstrate accurate radiogenic $^{87}Sr/^{86}Sr$ and naturally-invariant $^{84}Sr/^{86}Sr$-ratios, without any significant long-term trend. Not only high-[Sr] shark teeth, but also low-[Sr] human tooth enamel samples record accurate $^{84}Sr/^{86}Sr$-ratios, showing that Ca-argide/dimers are negligible and Kr corrections valid.

2) The external precision for $^{84}Sr/^{86}Sr$ in both solution and laser-ablation mode are essentially similar (±0.7 ‰; 2 SD), yet $^{87}Sr/^{86}Sr$ in laser-mode is about four times less reproducible (±0.075 ‰, 2 SD). While this is still satisfactory for many applications in view of the large natural $^{87}Sr/^{86}Sr$ variations, we attribute this deterioration mainly to slightly fluctuating on-peak ^{85}Rb baselines not uncommon for volatile Rb, which may occur despite best efforts to introduce minimal Rb during instrument setup. This becomes significant mainly when dealing with low(est)-Rb/Sr samples such as shark teeth, silicate minerals or carbonates; for the latter we obtain broadly similar long-term precision during *carbonate* LA-MC-ICPMS Sr-isotope analysis[54].

3) We advocate the *routine* reporting of the non-radiogenic, invariant $^{84}Sr/^{86}Sr$ ratio (if 'traditionally' $^{88}Sr/^{86}Sr$-normalized) for *all samples and standards* analyzed by LA-MC-ICPMS, which facilitates *routine* accuracy assessment of obtained data, akin to e.g. Hf-isotopes[32]. Given the significant potential from unaccounted spectral interferences for inaccurate LA-MC-ICPMS Sr-isotope data, this opportunity should not be omitted and Sr-data without accurate $^{84}Sr/^{86}Sr$ ratios could be considered unreliable.

4) Even though REE concentrations in modern or well-preserved fossil/archaeological bioapatite are exceedingly low (lowest-ppb range), doubly-charged REE (mainly Er, Yb) should be monitored at nominal half-mass(es), as any deviation from baseline values constitutes a simple yet powerful way to monitor the level of alteration in fossil samples.

5) We find no evidence for significant polyatomic interferences, neither Ca-argides/dimers (cf. accurate $^{84}Sr/^{86}Sr$ ratios), nor any significant $^{40}Ca^{31}P^{16}O$ at m/z=87. The presence of the latter is testable via mass scan experiments at (pseudo)high mass resolution, but no evidence of a minor peak (shoulder) at slightly higher mass was found using either FAR or SEM, even when plasma conditions were deliberately detuned to simulate very high ThO^+/Th^+-ratios. This is in line with the lower metal-(cation)-oxide bond strengths of Ca^+-O and P^+-O (and likely even more so for triatomic CaPO) that are known to be correlated with metal-oxide production rates[29].

6) In view of the moderately elevated $^{85}Rb/^{86}Sr$-ratios often typical of (bio)apatite, we focus on the accuracy of the ^{87}Rb correction. We constrain both the effective $^{85}Rb/^{87}Rb$-ratio in the presence of major Ca-P ions, as well as the extent of elemental Rb/Sr fractionation during laser-ablation, using matrix-matched phosphate glasses. The latter does not appear to have been sufficiently explored in previous LA-MC-ICPMS Sr-isotope analysis of (bio)apatite but is significant (~15 %), and in line with the strong volatility difference between Rb and Sr. Similar to the routine reporting of $^{84}Sr/^{86}Sr$ ratios, we propose that *LA-MC-ICPMS Sr-isotope data routinely include corresponding $^{85}Rb/^{86}Sr$-ratios.*

7) We showcase our LA-MC-ICPMS Sr methodology via a case study of human teeth from a medieval German mining site, characterized by fairly elevated $^{85}Rb/^{86}Sr$ ~0.005-0.009. One early and one late mineralizing molar of the same individual record highly variable intra/inter-enamel $^{87}Sr/^{86}Sr$ ratio profiles, while maintaining accurate invariant $^{84}Sr/^{86}Sr$. We finally validate the accuracy of the LA $^{87}Sr/^{86}Sr$ ratios via comparative TIMS-microsampling Sr-isotope data. However, there is a limit in the usefulness of any LA vs. TIMS data comparison, owing to the complex enamel mineralization process with differently condensed time-series across and along enamel. It is evident that in case of highly variable intra-tooth $^{87}Sr/^{86}Sr$ ratios, it is difficult to define equivalent sample volumes, which in our view needs to be acknowledged when assessing the reliability of such comparisons.

The outlined methodology allows reliable, simple and fast spatially-resolved Sr isotope analysis, applicable to high-time resolution studies in palaeoecology, archaeology/anthropology or any (geological) sciences, whose potential overall has insufficiently been explored so far.

5) Acknowledgements

We are indebted to Ashley Norris and Jarosław Wilczyński for their help with the modern shark teeth provision. We thank Jakub Bazarnik for his help with the chemical purification of the Ca-P solution. We are grateful to Stephan Klemme and Andy Carter for providing the STDP glasses and Durango apatite, respectively. Kurt Alt, Julia Bastin, David Evans and Mark Rauschkolb are thanked for help with various aspects of the Sulzburg work, as is Matthew Thirlwall for some assistance with TIMS analysis at RHUL. Special thanks are due to Luca Bondioli for the photograph in Fig. 1 and many discussions on enamel mineralization and histology. Funding from an internal IGS PAS grant (to RA) and EU FP7-REGPOT-2011-1 ('ATLAB') is most gratefully acknowledged. Thanks to Detlef Günther and Frank Vanhaecke for the invitation to contribute to JAAS' 30th anniversary volume. The comments of two anonymous reviewers helped to clarify our arguments and are gratefully acknowledged.

References

1 1. B. L. A. Charlier, C. Ginibre, D. Morgan, G. M. Nowell, D. G. Pearson, J. P. Davidson and C. J. Ottley, *Chem. Geol.*, 2006, **232**, 114-133.
2 2. W. Müller, D. Aerden and A. N. Halliday, *Science*, 2000, **288**, 2195-2198.
3 3. J. N. Christensen, A. N. Halliday, D. C. Lee and C. M. Hall, *Earth Planet. Sci. Lett.*, 1995, **136**, 79-85.
4 4. S. Burla, F. Oberli, U. Heimhofer, U. Wiechert and H. Weissert, *Terr. Nova*, 2009, **21**, 401-409.
5 5. F. C. Ramos, J. A. Wolff and D. L. Tollstrup, *Geology*, 2005, **33**, 457-460.
6 6. M. McCulloch, M. Cappo, J. Aumend and W. Müller, *Marine and Freshwater Research*, 2005, **56**, 637-644.
7 7. J. Woodhead, S. Swearer, J. Hergt and R. Maas, *J. Anal. At. Spectrom.*, 2005, **20**, 22-27.
8 8. T. Waight, J. Baker and D. Peate, *Int. J. Mass Spectrom.*, 2002, **221**, 229-244.

9. P. Z. Vroon, B. van der Wagt, J. M. Koornneef and G. R. Davies, *Analytical and Bioanalytical Chemistry*, 2008, **390**, 465-476.
10. M. Bizzarro, A. Simonetti, R. K. Stevenson and S. Kurszlaukis, *Geochim. Cosmochim. Acta*, 2003, **67**, 289-302.
11. M. S. A. Horstwood, J. A. Evans and J. Montgomery, *Geochim. Cosmochim. Acta*, 2008, **72**, 5659-5674.
12. A. Simonetti, M. R. Buzon and R. A. Creaser, *Archaeometry*, 2008, **50**, 371-385.
13. S. R. Copeland, M. Sponheimer, P. J. le Roux, V. Grimes, J. A. Lee-Thorp, D. J. de Ruiter and M. P. Richards, *Rapid Commun. Mass Spectrom.*, 2008, **22**, 3187-3194.
14. V. Balter, P. Telouk, B. Reynard, J. Braga, F. Thackeray and F. Albarede, *Geochim. Cosmochim. Acta*, 2008, **72**, 3980-3990.
15. D. E. Harlov, *Elements*, 2015, **11**, 171-176.
16. R. A. Bentley, *Journal of Archaeological Method and Theory*, 2006, **13**, 135-187.
17. W. Müller, H. Fricke, A. N. Halliday, M. T. McCulloch and J. A. Wartho, *Science*, 2003, **302**, 862-866.
18. L. Bondioli, P. F. Rossi and W. Müller, *Geochim. Cosmochim. Acta*, 2009, **73**, A136-A136.
19. J. Montgomery, J. A. Evans and M. S. A. Horstwood, *Environmental Archaeology*, 2010, **15**, 32-42.
20. C. FitzGerald, S. Saunders, L. Bondioli and R. Macchiarelli, *Am J Phys Anthropol*, 2006, **130**, 179-189.
21. R. H. Steiger and E. Jäger, *Earth Planet. Sci. Lett.*, 1977, **36**, 359-362.
22. W. Müller, M. Shelley, P. Miller and S. Broude, *Journal Analytical Atomic Spectrometry*, 2009, **24**, 209-214.
23. E. A. Hinz and M. J. Kohn, *Geochim. Cosmochim. Acta*, 2010, **74**, 3213-3231.
24. F. Vanhaecke, C. Vandecasteele, H. Vanhoe and R. Dams, *Microchimica Acta*, 1992, **108**, 41-51.
25. S. F. Durrant, *Fresenius J. Anal. Chem.*, 1994, **349**, 768-771.
26. H. H. Cornehl, R. Wesendrup, M. Diefenbach and H. Schwarz, *Chemistry – A European Journal*, 1997, **3**, 1083-1090.
27. D. K. Bohme, Ion Chemistry Laboratory - Thermodynamics and Physical Properties Database, http://www.chem.yorku.ca/profs/bohme/research/tpp__MAIN.html, (accessed September 2015, 2015).
28. Y.-R. Luo and J. A. Kerr, in *CRC handbook of chemistry and physics*, ed. D. R. Lide, CRC press, 2005, vol. 86, pp. 9-54 - 59-63.
29. A. J. R. Kent and C. A. Ungerer, *J. Anal. At. Spectrom.*, 2005, **20**, 1256-1262.
30. D. Schröder, H. Schwarz and S. Shaik, in *Metal-Oxo and Metal-Peroxo Species in Catalytic Oxidations*, ed. B. Meunier, Springer Berlin Heidelberg, 2000, vol. 97, ch. 4, pp. 91-123.
31. J. Lewis, C. D. Coath and A. W. G. Pike, *Chem. Geol.*, 2014, **390**, 173-181.
32. T. M. Harrison, J. Blichert-Toft, W. Müller, F. Albarede, P. Holden and S. J. Mojzsis, *Science*, 2005, **310**, 1947-1950.
33. W. Müller, N. S. Mancktelow and M. Meier, *Earth Planet. Sci. Lett.*, 2000, **180**, 385-397.
34. K. P. Jochum, U. Weis, B. Stoll, D. Kuzmin, Q. C. Yang, I. Raczek, D. E. Jacob, A. Stracke, K. Birbaum, D. A. Frick, D. Gunther and J. Enzweiler, *Geostand. Geoanal. Res.*, 2011, **35**, 397-429.
35. S. Klemme, S. Prowatke, C. Munker, C. W. Magee, Y. Lahaye, T. Zack, S. A. Kasemann, E. J. A. Cabato and B. Kaeser, *Geostand. Geoanal. Res.*, 2008, **32**, 39-54.
36. J. M. McArthur, R. J. Howarth and T. R. Bailey, *J. Geol.*, 2001, **109**, 155-170.
37. K. W. Alt, B. Lohrke, R. Brenn, W. Müller, M. Rauschkolb and H. Steuer, *Die mittelalterliche Bergbaubevölkerung des 12. Jahrhunderts von Sulzburg, Kr. Breisgau-Hochschwarzwald. Anthropologische und archäometrische Studien.*, VML Verlag Leidorf, 2008.
38. K. W. Alt, C. P. Adler, C. H. Buitrago-Tellez and B. Lohrke, *Int. J. Osteoarchaeol.*, 2002, **12**, 442-448.
39. M. F. Thirlwall, *Chem. Geol.*, 1991, **94**, 85-104.
40. F. C. Ramos, J. A. Wolff and D. L. Tollstrup, *Chem. Geol.*, 2004, **211**, 135-158.
41. Y.-H. Yang, F.-Y. Wu, J.-H. Yang, D. M. Chew, L.-W. Xie, Z.-Y. Chu, Y.-B. Zhang and C. Huang, *Chem. Geol.*, 2014, **385**, 35-55.
42. L. J. Moens, F. F. Vanhaecke, D. R. Bandura, V. I. Baranov and S. D. Tanner, *J. Anal. At. Spectrom.*, 2001, **16**, 991-994.
43. S. Weyer and J. Schwieters, *Int. J. Mass Spectrom.*, 2003, **226**, 355-368.
44. R. Brogioli, B. Hattendorf, J. Koch, H. Wiltsche, L. Flamigni and D. Günther, *Analytical and Bioanalytical Chemistry*, 2011, **399**, 2201-2209.
45. E. Catanzaro, T. Murphy, E. Garner and W. Shields, *J. Res. Natl. Bur. Stand. A*, 1969, **73**, 511-516.
46. J. I. Kimura, T. Takahashi and Q. Chang, *J. Anal. At. Spectrom.*, 2013, **28**, 945-957.
47. V. Balter, J. Braga, P. Telouk and J. F. Thackeray, *Nature*, 2012, **489**, 558-560.
48. K. Lodders, *The Astrophysical Journal*, 2003, **591**, 1220.
49. S. M. Eggins, L. P. J. Kinsley and J. M. G. Shelley, *Appl. Surf. Sci.*, 1998, **129**, 278-286.
50. W. Müller, unpublished data.
51. S. J. Alqahtani, M. Hector and H. Liversidge, *Am J Phys Anthropol*, 2010, **142**, 481-490.
52. M. Wormuth, MSc (Diplom), Georg-August-Universität Göttingen, 2000.
53. R. A. Bentley and C. Knipper, *Archaeometry*, 2005, **47**, 629-644.
54. W. Müller and R. Anczkiewicz, unpubl. data.